Progress In Electromagnetics Research, Vol. 114, 129–144, 2011

PLANAR MULTIBAND BANDPASS FILTER WITH MULTIMODE STEPPED-IMPEDANCE RESONATORS

Y.-C. Chiou

Department of Electrical and Computer Engineering
University of California at San Diego, USA

J.-T. Kuo

Department of Electronic Engineering
Chang Gung University, Taoyuan, Taiwan

Abstract—Planar multiband bandpass filters are implemented based on the versatile multimode stepped-impedance resonators (SIRs). The resonant spectrum of a SIR can be calculated as functions of the length ratios for various impedance ratios of the high- and low-impedance sections. Thus, by properly selecting the geometric parameters and designing the input/output coupling structure, the SIRs are feasible to realize multiband multimode filters. Using a single SIR, a dual-mode dual-band, a dual-mode triple-band or a hybrid dual-/triple-mode dual-band bandpass filter can be realized. Emphasis is also placed on designing specified ratios of center frequencies and fractional bandwidths of the passbands. To extend the design flexibility, extra shunt open stubs are used to adjust the ratio of the passband frequencies. In addition, sharpness of the transition bands is improved by designing the input/output stages. Simulation results are validated by the measured responses of experimental circuits.

1. INTRODUCTION

Recently, wireless communication systems capable of processing signals in different frequency bands have become more and more popular. Multiband antennas [1, 2] and filters [3–9] have been investigated with new synthesis methods or innovative designs. In [3], the multiband bandpass filter is realized by either placing transmission

Received 20 January 2011, Accepted 21 February 2011, Scheduled 23 February 2011
Corresponding author: Jen-Tsai Kuo (jtkuo123@mail.cgu.edu.tw).

zeros within the passband of a wideband filter or employing higher order resonances. Based on the conventional coupling matrices, extended designs of dual- and triple-band filters are demonstrated. In [4], a frequency transformation is developed for determining the poles and zeros of triple-band bandpass filters. In [5], a rigorous synthesis procedure of dual-band bandpass filters in parallel-coupled and in-line configurations is proposed. In [6], coupling structures are presented to achieve dual- and triple-band functions with both Chebyshev and quasi-elliptic frequency responses without a significant increase in circuit size. In [7], based on the substrate integrated structure technology, synthesis and design techniques are proposed for dual- and triple-passband filters with Chebyshev and quasi-elliptic responses. In [8], the two passbands can be designed individually and several transmission zeros can be created to improve the frequency selectivity. In [9], a folded stepped-impedance resonator (SIR) is used as a basic block for a new implementation of dual-band filters.

It is noted that the multiband filters in [3–9] each resonator contributes one transmission pole in one passband. Thus, for example, a 12-pole passband will involve 12 resonators [4]. Recently, planar multimode bandpass filters have become a very popular topic [10–16]. A multimode resonator possesses multi-resonance property so that higher order circuits can be synthesized with fewer resonators, leading to circuit area reduction and improved rejection in stopband for bandpass filters. In [10, 11], triple- or quadruple-mode resonators are proposed for filter design. In [12], broadband filters are realized by incorporating the leading three resonances of a SIR. In [13, 14], broadband and ultra-wideband bandpass filters are developed with single and coupled SIRs. A ninth-order quasi-Chebyshev filter is synthesized by three resonating elements. In [15], an ultra-wideband bandpass filter with a wide upper stopband is achieved by using modified multimode resonator with stepped-impedance stubs. In [16], multimode bandpass filter is designed with a single SIR tapped with several open stubs. A cascade of such multimode resonators is also devised to double the filter order for improving the rejection levels in upper stopband. Note that the circuits in [10–16] consider only a single passband.

Several new multiband filters have been proposed based on multimode resonators [17–20]. In [17], a novel compact dual-mode ring resonator is developed with adjustable second passband for dual-band applications. The circuit, unfortunately, shows high insertion losses in both passbands and the two bandwidths can hardly be adjusted. In [18], the dual-band characteristic is achieved by configuring dual-mode resonators in different dielectric layers. In [19], a dual-band filter is designed using a multilayer approach including a reflector cavity and dual-mode resonators. Note that the circuits in [17–19], however, are limited to dual-mode dual-band applications. In [20], a tri-band filter is presented using tri-mode T-shaped branches connected by $\lambda/4$-sections. To realize different bandwidths for each, the admittance slope of each resonating mode is set as required. The dimension of each branch is solved by a genetic algorithm followed by an optimization.

In this paper, we aim at establishing a systematic procedure for synthesizing planar multiband filters on the basis of single or coupled multimode SIRs. Each SIR is treated as a multimode cavity that can contributes two or three resonances in different frequency bands. Based on the synthesis procedure in [11], dual-mode dual-band, dual-mode triple-band and hybrid dual-/triple- mode dual-band filters are realized with quasi-Chebyshev passbands. To this end, the impedance and length ratios of the SIRs are properly designed based on the resonant spectrum in readiness. Next, design graphs related to circuit bandwidth and frequency ratio between each band are investigated. The input/output coupling structures are devised to meet the bandwidth requirements of each band. Finally, four circuits with either a single SIR or two cascaded SIRs are implemented and measured for demonstration.

2. SIRS AS BUILDING BLOCKS

The resonant frequencies of a SIR in Fig. 1 can be calculated by two transcendental equations, e.g., [11]. Let $R = Z_2/Z_1$ be the impedance ratios, and θ_1 and θ_2 be the electrical lengths of the sections with characteristics impedances Z_1 and Z_2, respectively. Fig. 2 plots the resonant frequencies f_k against the length ratio $u = \theta_2/(\theta_1 + \theta_2)$ for the first (f_1) through the sixth higher order mode (f_6) for $R = 2$, 6 and 10. The resonant frequencies are normalized with respect to that of the fundamental resonance of a SIR with $R = 1$. In this study, only $0.5 \leq u \leq 1.0$ is of interest. This is because that when $u < 0.5$, the f_2/f_1 ratio is increased as u is decreased, as indicated in Fig. 2

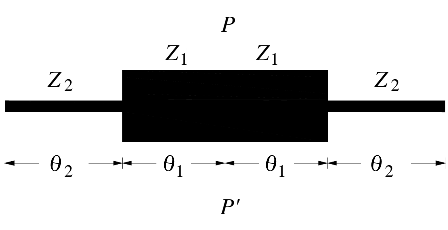

Figure 1. Geometry of a multimode SIR.

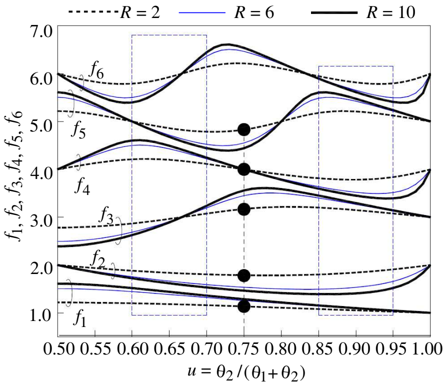

Figure 2. Normalized resonant frequencies of the SIR in Fig. 1.

of [13]. An increased f_2/f_1 ratio means the distance between these two resonances is increased. Thus, it is not suitable for dual- or multi-mode design, since the bandwidth will be too large to be synthesized. Based on the resonant characteristics shown in Fig. 2, the SIR is capable of constituting a building block for design of multimode multiband filter. When $u = 0.75$, for example, the SIR has five resonances (shown in black dots) in two groups before f_6. In the first group, the two resonances at f_1 and f_2 can be used for a dual-mode passband at a center frequency $f_{o1} = (f_1 + f_2)/2$ and three resonances at f_3, f_4 and f_5 in the second group can be employed to construct a triple-mode passband at $f_{o2} = (f_3 + f_5)/2$. It can be validated that when $u = 0.75$, $f_4 = (f_3 + f_5)/2$. Thus, $f_{o2} = f_4$. Note that the circuit will show a spurious peak at f_6, if it is not used as the third passband. Similarly, when $u = 0.9$ is chosen, the SIR can be used to synthesize a triple-band filter at center frequencies $f_{o1} = (f_1+f_2)/2$, $f_{o2} = (f_3+f_4)/2$ and $f_{o3} = (f_5 + f_6)/2$, and each passband will have a dual-mode response.

3. MULTIMODE MULTIBAND FILTERS

In design of a multi-passband filter with multimode SIRs, the tuning ranges of the ratios of the passband frequencies and their bandwidths are controlled by the resonant characteristics shown in Fig. 2. Thus, these passband specifications will determine the geometric parameters of the SIR. Thus, in this section, design graphs are plotted for ratios of the center frequencies and bandwidths. Finally, an adequate input/output coupling structure is devised to carry out the desired passbands.

3.1. Determination of Fractional Bandwidth

For the mth passband, let Δ_m and f_{om} be respectively the fractional bandwidth and the center frequency, and f_{nm} be the nth resonance frequency of the SIR. For instance, when $u = 0.9$, the resonances at $f_1 \sim f_6$ are grouped into three passbands of two modes so that they can be rewritten as f_{11}, f_{21}, f_{12}, f_{22}, f_{13} and f_{23}, respectively. The fractional bandwidth Δ_m can be written as [11]

$$\Delta_m = 2\frac{f_{nm} - f_{om}}{x_n \times f_{om}} \tag{1}$$

where x_n is the nth root of the ith-order Chebyshev polynomial of the first kind, i.e.,

$$x_n = \cos\left(\frac{2i+1-2n}{2i}\pi\right), \quad n = 1, 2, \ldots, i. \tag{2}$$

In our design, dual- and triple-mode passbands will have $i = 2$ and 3, respectively. In accordance with (1) and (2), the Δ_m value can be easily calculated.

3.2. Input/Output Coupling

Coupling design between the input/output feeders and the end resonators is a critical issue for the multiband multimode filter to be synthesized [Fig. 4, 14]. Herein, the parallel-coupled structure is used as the feeders. For the multimode design with a single passband in [11], the external quality factor Q (Q_{ext}) is given as

$$Q_{extm} = \frac{2\pi Z_o}{Z_{oem} - Z_{oom}} \tag{3}$$

where Z_o is reference port impedance and Z_{oem} and Z_{oom} are the modal characteristic impedances of the coupled-line stage at the mth passband. Note that the values of Z_{oem} and Z_{oom} can be determined by Table 10.02-1 in [21], and hence the line width and gap size of the stage can be calculated. Note that if both Z_{oem} and Z_{oom} are determined by the fractional bandwidth Δ_m, then different passbands may require different line widths and gap sizes. Moreover, the line width is a geometric parameter of the SIR and has been fixed by the designated resonant frequencies. Therefore, it is a challenge to simultaneously fulfill the coupling requirements of all passbands. In (9) of [11], the loaded quality factor (Q_L) of a coupled-line section has been derived for a broadband application. On the basis of Sec. 11.02 and 11.03 of [21], the loaded quality factor of a coupled stage for each passband

(Q_{Lm}) can be further derived and involved with its external quality factor (Q_{em}):

$$Q_{em} = Q_{Lm} V_{om} \tag{4}$$

where $Q_{Lm} = f_{om}/\Delta f_m$, Δf_m denotes the half-power bandwidth of the coupled-line stage for the mth passband, and V_{om} is the voltage standing wave ratio (VSWR) and 1/VSWR at the midband when the stage is undercoupled and overcoupled, respectively. When the stage is critically coupled, $V_{om} = 1$ and $Q_{em} = Q_{Lm}$.

To investigate the coupling property of a coupled-line section in Fig. 3(a), Fig. 3(b) investigates simulated responses of such a stage with overcoupled, critically coupled and undercoupled conditions for the first three passbands. When the coupled-line stage is overcoupled, within each passband there are two transmission poles due to the strong coupling between the input and output ports [10, 11, 21] and the passband has a relatively wide bandwidth. When the stage

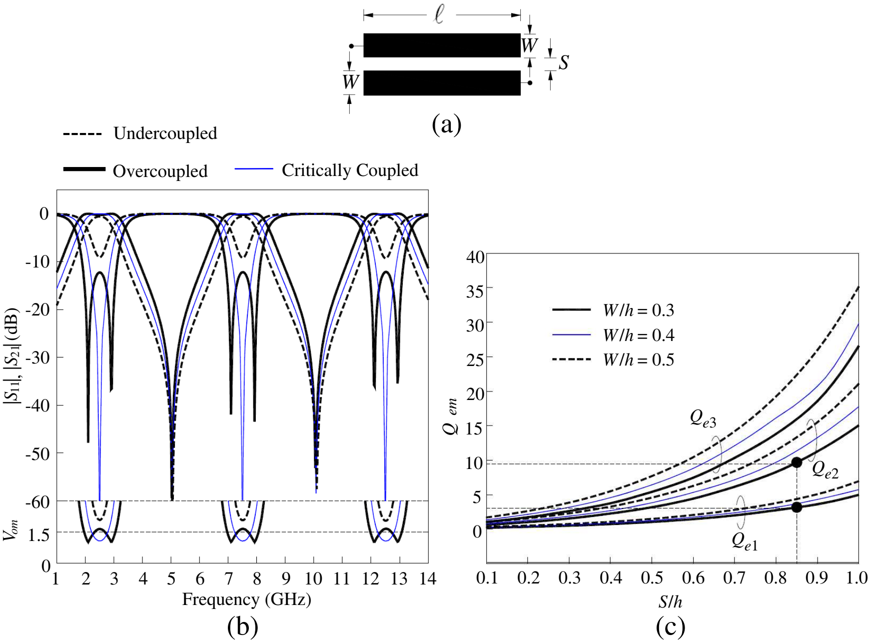

Figure 3. (a) A coupled-line stage. (b) Simulated responses of the coupled-line stage. Circuit dimensions: $W = 0.25$, $\ell = 29.78$ and $S = 0.15$, 0.278 and 0.45 for overcoupled, critically coupled and undercoupled conditions, respectively. All lengths are in mm. (c) Simulated Q_{em} of the coupled-line stages versus S/h.

Table 1. Simulated values of Q_{lm}, V_{om} and Q_{em} of the coupled-line stage for overcoupled, critically coupled and undercoupled conditions in Fig. 3(b).

Condition	Q_{L1}	Q_{L2}	Q_{L3}	V_{o1}	V_{o2}	V_{o3}	Q_{e1}	Q_{e2}	Q_{e3}
Overcoupled	1.39	4.17	7.02	1.64	1.65	1.66	0.85	2.53	4.23
Critically coupled	1.88	5.6	9.33	1.00	1.00	1.00	1.88	5.6	9.33
Undercoupled	2.5	7.5	12.5	2.08	2.06	2.04	5.2	15.5	25.5

is critical coupled, it has a perfect input matching at the design frequencies. Table 1 summaries the simulated values of Q_{Lm}, V_{om} and Q_{em} in Fig. 3(b), where $W/h = 0.492$ and $S/h = 0.295$, 0.547, and 0.886 for the overcoupled, critically coupled and undercoupled conditions, respectively. For each condition, since all absolute half-power bandwidths of the first three passbands are approximately the same, one can see that both Q_{Lm} and Q_{em} increase as m increases. Fig. 3(c) draws the simulated Q_{em} of the coupled-line stage against the gap size S/h. As S/h is increased, all Q_{em} values increase. It is because that a weaker input/output coupling is usually accompanied with a smaller fractional bandwidth so that Q_{em} becomes higher. Since narrower coupled-line has stronger coupling, leading to a larger bandwidth, all Q_{em} values decrease as W/h is decreased. Note that the coupled-line section is overcoupled for all W/h when $S/h < 0.5$. Here, the circuit substrate has $\varepsilon_r = 2.2$ and thickness $h = 0.508$ mm. The software package IE3D [22] is used for circuit simulation.

3.3. Dual-Mode Dual-Band Bandpass Filter

A single SIR can be used to design a dual-mode dual-band bandpass filter. Based on Fig. 2, by choosing $0.6 \leq u \leq 0.7$, one can synthesize the first passband with the resonances at f_1 and f_2, and the second by those at f_4 and f_5. The resonance at f_3 is purposely bypassed. It may become a spurious if no suppression approach [23, 24] is applied. According to the notation given in (1), f_1, f_2, f_4 and f_5 are rewritten as f_{11}, f_{21}, f_{12}, f_{22} in (3), respectively. Fig. 4 plots the tuning ranges of the fractional bandwidths Δ_1 and Δ_2 versus R for various u values. The results are obtained by invoking the resonant characteristics of the SIRs in Fig. 2 and calculated by (3) and (4). When R is increased, both bandwidths Δ_1 and Δ_2 decrease, since for example the space between f_{11} and f_{21} decreases. These curves reveal that the two bandwidths are determined at the same time when R and u are given. It can be observed from Fig. 2 that f_6 moves to a higher frequency as u is close

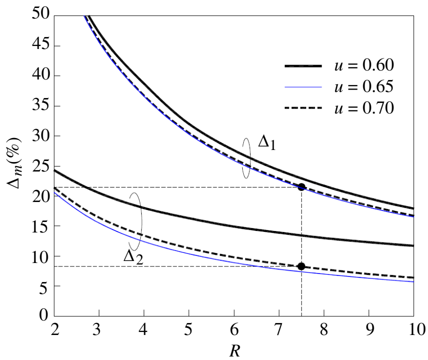

Figure 4. Fractional bandwidths of the dual-band SIR filter versus R for various u values.

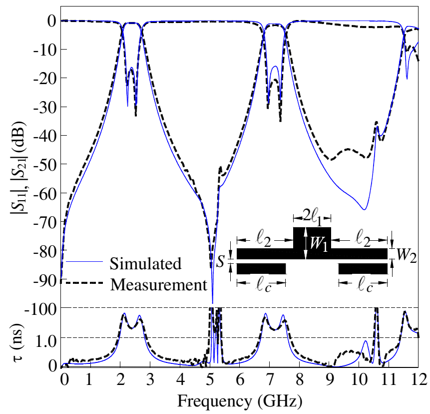

Figure 5. Simulated and measured responses of the dual-mode dual-band bandpass filter. Circuit dimensions: $W_1 = 5.63$, $W_2 = 0.167$, $\ell_1 = 9.22$, $\ell_2 = 23.6$, $\ell_c = 24$, $S = 0.435$. All are in mm.

to 0.7. It is a favorable choice for a relative wide upper rejection band if $u = 0.7$ is used.

Figure 5 plots the simulation and measured responses of the dual-mode dual-band filter based on a SIR with $R = 7.5$. The center frequencies $f_{o1} = 2.35$ GHz and $f_{o2} = 7.15$ GHz, ripple $= 0.1$ dB and the bandwidths $\Delta_1 = 20\%$ and $\Delta_2 = 8\%$. Based on (2), the values of Q_{ext1} and Q_{ext2} are 3.05 and 9.18, respectively. Consequently, the value of S/h could be readily obtained if W/h is determined on the basis of Fig. 3(b). For $W/h = 0.3$, for example, the value of $S/h = 0.85$. The measurement shows that the in-band insertion losses are only 0.85 dB and 1.1 dB at f_{o1} and f_{o2}, respectively. The resonance at $f_3 = 4.95$ GHz is suppressed by the inherent transmission zero created by the input/output coupled stage [23]. Between the two passbands, the filter shows a very good rejection. In addition, a 40-dB rejection level is extended up to 10.5 GHz. The group delays of two passbands vary from 1.25 ns to 1.8 ns. It is noted that the group delay responses have relatively larger variations near the frequency of the transmission zero. Good agreement between simulation and measured results can be observed.

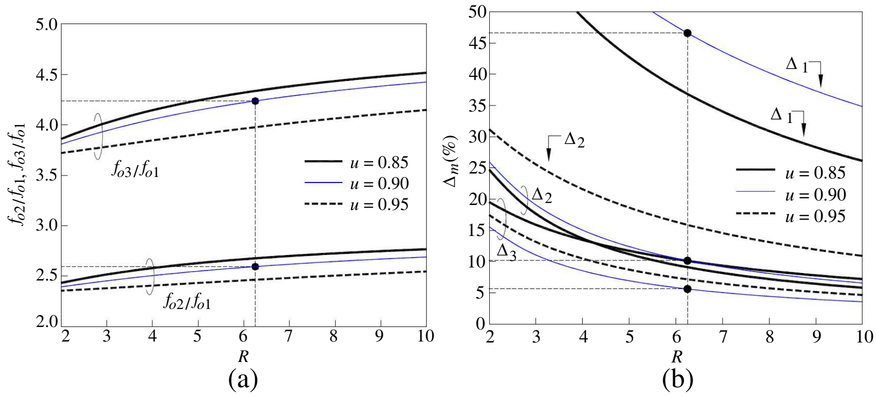

Figure 6. (a) Center frequency ratios (f_{om}/f_{o1}) and (b) fractional bandwidth (Δ_m) graph of the triple-band filter versus R for various u values.

3.4. Dual-Mode Triple-Band Filter

The second demonstration is a dual-mode triple-band filter with controllable bandwidths and ratios of the center frequencies. Based on the data in Fig. 2, the u values from 0.85 to 0.95 can be chosen to meet this purpose. Three pairs of resonances (f_{2i-1} and f_{2i}, $i = 1$, 2 and 3) constitute the three passbands. Fig. 6(a) depicts the ratios of their center frequencies (f_{om}/f_{o1}, $m = 2$ and 3). The ratio f_{o2}/f_{o1} moves from 2.35 to 2.76 and f_{o3}/f_{o1} from 3.75 to 4.51 when R is varied from 2 to 10. Both f_{o2}/f_{o1} and f_{o3}/f_{o1} ratios decrease as u is increased from 0.85 to 0.95. Fig. 6(b) plots the three bandwidths of the triple-band filter versus the impedance ratio R for $u = 0.85$, 0.9 and 0.95. It is interesting to note that Δ_1 is much larger than Δ_2 and Δ_3. When $u = 0.95$, $\Delta_1 > 50\%$ so that the curve is not shown here. Again, each bandwidth decreases when R is increased.

Figure 7(a) shows the layout of the dual-mode triple-band filter using only one SIR, and Fig. 7(b) shows the photograph of the experimental circuit. A folded coupled-line stage is used as the input/output structure. To investigate its coupling characteristics, Fig. 7(c) plots its simulated $|S_{21}|$ responses with $\ell_{c1} = 19.65 \sim 22.65\,\text{mm}$ while $\ell_{c1} + \ell_{c2} = 26\,\text{mm}$. The three transmission zeros, fractional bandwidths and ratios of center frequencies can be simultaneously adjusted by tuning the ℓ_{c1}. One can observe that the second transmission zero is approximately twice the first one. This means both zeros are generated by the coupled-line coupler ℓ_{c1} [23]. Similarly, the third one is attributed to the coupled-line ℓ_{c2}. On the

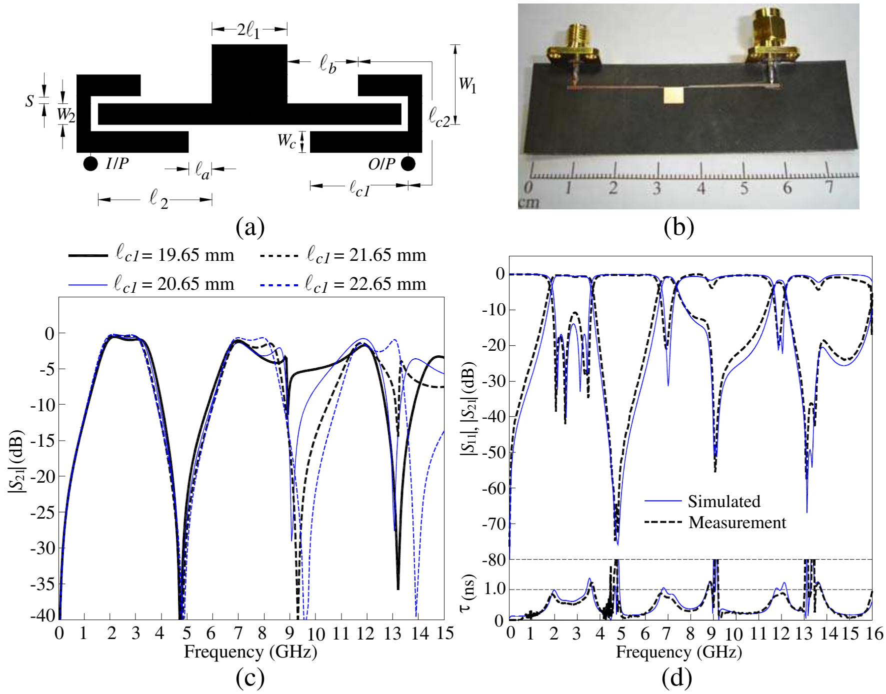

Figure 7. (a) Circuit layout. (b) Photograph of the experimental dual-mode triple-band bandpass filter. (c) Simulated frequency responses of the folded coupled-line stage, where $W_2 = W_c = 0.15$, $\ell_2 = 23.45$, $S = 0.15$, $\ell_{c1} + \ell_{c2} = 26$, $W_1 = \ell_1 = \ell_a = \ell_b = 0$. All are in mm. (d) Simulation and measured responses and Circuit dimensions: $W_1 = 4.16$, $W_2 = W_c = 0.15$, $\ell_1 = 2.39$, $\ell_2 = 23.45$, $\ell_{c1} = 19.9$, $\ell_{c2} = 2.89$, $\ell_a = 1.45$, $\ell_b = 20.2$, $S = 0.15$. All are in mm.

basis of a design procedure similar to that presented in Sec. 3.3, sufficient coupling can be achieved for the three designated bands by properly selecting the tap positions of input/output ports. Fig. 7(d) depicts the simulation and measured results of the filter. The SIR has $R = 6.25$ and $u = 0.9$. From the dashed lines in Fig. 6, $f_{o2}/f_{o1} = 2.6$, $f_{o3}/f_{o1} = 4.23$, $\Delta_1 = 46.6\%$, $\Delta_2 = 10.2\%$, and $\Delta_3 = 5.6\%$. The measured insertion losses at f_{o1}, f_{o2} and f_{o3} are only 0.6 dB, 0.8 dB and 1.8 dB, respectively. All the in-band return losses are below 14 dB. In the first passband, two extra transmission poles can be observed, since the input/output stages are overcoupled. It is worth mentioning that the transmission zeros attributed to the coupled section 5 GHz, 9 GHz and 13 GHz which significantly improve the performances of the filter in the transition bands. The largest variation of group delays within three passbands is only 0.8 ns. The measurement results have good agreement with the simulation counterparts.

3.5. Hybrid Dual-/Triple-Mode Dual-Band Filter

As shown in Fig. 2, when $u = 0.75$ the distance between f_3 and f_4 is very close to that of f_4 and f_5. Accordingly, it seems to be a proper choice to devise a filter with two passbands; one is dual-mode with the resonances f_1 and f_2 and the other is triple-mode band with f_3, f_4 and f_5. Fig. 8(a) investigates the variations of the bandwidths and f_{o2}/f_{o1} against R. The f_{o2}/f_{o1} ratio moves to a higher value while both Δ_1 and Δ_2 move down to lower values when R is increased. The Δ_1 value shifts down more quickly than Δ_2 and $\Delta_1 < \Delta_2$ when $R > 4.37$. Fig. 8(b) presents the simulated and measured results of the hybrid dual-/triple-mode dual-band filter. Again, the second zero is twice that of the first one. Therefore, one can readily conclude that both zeros are created by the input/output three-line coupler. The circuit structure is similar to the filter shown in Fig. 7(a). The R value of the SIR is 9.6, and all other geometric parameters are also given. The two center frequencies $f_{o1} = 2.2$ GHz and $f_{o2} = 6.7$ GHz and the two fractional bandwidths $\Delta_1 = 18.89\%$ and $\Delta_2 = 25.96\%$. In the passbands at f_{o1} and f_{o2}, the measured return losses are 16 dB

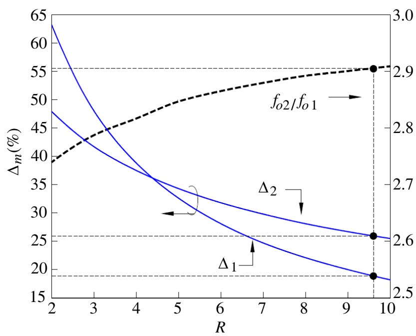

(a)

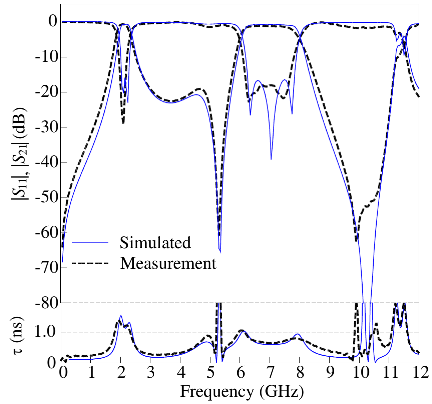

(b)

Figure 8. (a) Variations of Δ_m and f_{o2}/f_{o1} versus R. (b) Simulation and measured results of the hybrid dual-/triple-mode dual-band bandpass filter. Circuit dimensions: $W_1 = 7.18$, $W_2 = 0.15$, $\ell_1 = 7.11$, $\ell_2 = 23.55$, $\ell_{c1} = 13.1$, $\ell_{c2} = 9.1$, $\ell_a = 7.5$, $\ell_b = 17.35$, $S = 0.13$. All are in mm.

and 18 dB, respectively, and both in-band insertion losses are only 0.7 dB. It is worth mentioning that the first passband has a better phase characteristic than the second one, since that the first passband has less resonant modes than the second [11]. Note that $u = 0.6$ (see Fig. 2) could also be an alternative option to carry out a hybrid dual-/triple-mode dual-band filter. However, since $f_3 = 1.62 f_{o1} (R = 9.6)$ could not be directly eliminated by inherent zeros of coupled section, extra efforts such as slots etched on the ground plane [25] may be necessary to suppress the resonance at f_3.

3.6. Higher Order Dual-Band Filter with a Cascade of Hybrid Dual-/Triple-Mode Resonators

Synthesis of a dual-band filter of higher order with a cascade of two coupled hybrid dual-/triple-mode SIRs is also studied. Fig. 9(a) shows half of its layout since the whole circuit is symmetric. The two SIRs are identical and designed to have $R = 10$ and $u = 0.75$. The open stubs, line width W_s and length ℓ_s, tapped to the resonator are used

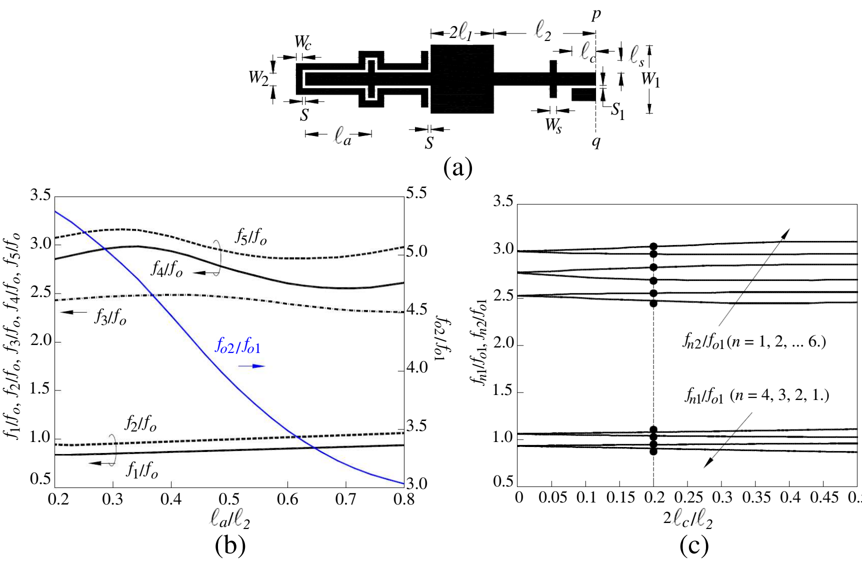

Figure 9. Design and results of coupled hybrid dual-/triple-mode dual-band bandpass filters. (a) Half of the circuit layout. (b) Normalized resonance frequencies f_k/f_o and center frequency ratio f_{o2}/f_{o1} with various ℓ_a/ℓ_2. (c) Mode graph versus $2\ell_c/\ell_2$ with $\ell_a = 20.5$. Circuit dimensions: $W_1 = 8.18$, $W_2 = 0.15$, $W_s = 0.5$, $\ell_1 = 12.06$, $\ell_2 = 35.55$, $\ell_s = 2.1$, $S = 0.15$, $S_1 = 0.27$. All are in mm.

to adjust the resonant frequencies. The two center frequencies change with different amounts by the shunt stubs so that the ratio of the center frequencies of the passbands f_{o2}/f_{o1} is also adjusted. The tap position is referred as the distance ℓ_a. For an isolated resonator with tapped open stubs, Fig. 9(b) plots the normalized resonant frequencies f_k/f_o and ratio of the two center frequencies f_{o2}/f_{o1} versus ℓ_a/ℓ_2, where f_o denotes the resonance frequency of an uniform resonator, i.e., $R = 1$. Here, both f_1/f_o and f_2/f_o slightly shift to higher frequencies as ℓ_a/ℓ_2 is increased. The distances among the ratios $f_3/f_o \sim f_5/f_o$ also vary as ℓ_a/ℓ_2 is changed. As ℓ_a/ℓ_2 is changed from 0.2 to 0.4, for example, the f_4/f_o moves to a higher value, while f_3/f_o almost maintains as the same level. It is noted that ratio of the two center frequencies f_{o2}/f_{o1} changes from 3.03 to 5.37. This indicates that this circuit possesses a wider frequency tuning range than the circuit without stubs shown in Fig. 8(a). Fig. 9(c) investigates the split-off of the resonance peaks of the coupled SIRs with various $2\ell_c/\ell_2$ ($2\ell_c$ is the coupling length). One can see that both have the similar results. When $2\ell_c/\ell_2$ increases, the distances between the resonances of the two bands increase, as expected. Finally, $2\ell_c/\ell_2 = 0.2$ are chosen for our demonstration.

Figure 10(a) illustrates the simulation and measurement results.

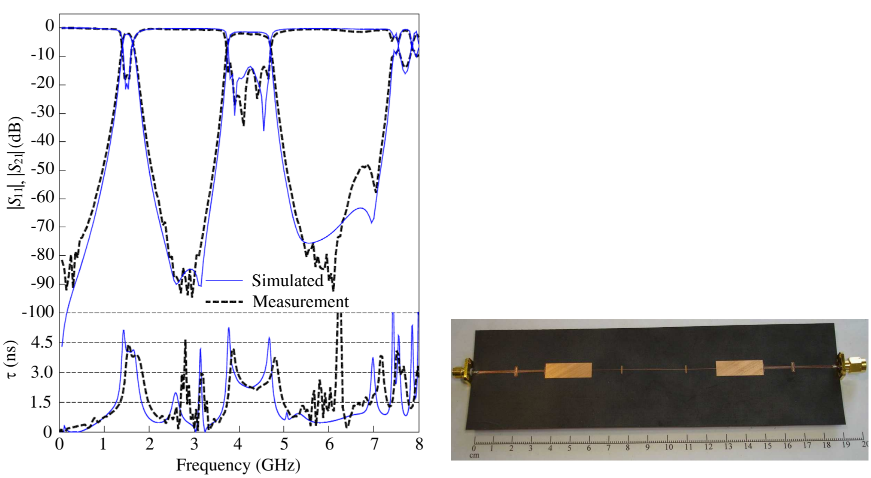

(a) (b)

Figure 10. Simulation and measured responses of coupled bandpass filter with hybrid dual-/triple-mode dual-band SIRs. (b) Circuit photo of (a). Circuit dimensions: $W_1 = 8.18$, $W_2 = 0.15$, $W_s = 0.5$, $\ell_1 = 12.06$, $\ell_2 = 35.55$, $\ell_a = 20.5$, $\ell_c = 3.5$, $\ell_s = 2.1$, $S = 0.15$, $S_1 = 0.27$. All are in mm.

The input/output coupling uses the three-line microstrip configuration [26] for coupling enhancement. The two center frequencies are measured at $f_{o1} = 1.5$ GHz and $f_{o2} = 4.1$ GHz. The measurement shows that in-band insertion losses at f_{o1} and f_{o2} are approximately 1.4 dB, and the return losses are 16 and 20 dB, respectively. Not only the transition bands show good roll-off rates, but also the best rejection between two passbands is better than 80 dB. The group delay in the first passband varies from 4 ns to 5 ns, while that in the second is from 2.2 ns to 5.3 ns. Fig. 10(b) is the photograph of the experimental circuit.

4. CONCLUSION

Multiband filters are synthesized and designed with multimode SIRs. Based on the modal resonant spectrum of the SIR, dual-mode dual-band, dual-mode triple-band and hybrid dual-/triple-mode dual-band bandpass filters are realized by either a single or two coupled SIRs. Both the ratio of the passband frequencies and the bandwidth design graphs are provided for circuit synthesis. Open stubs tapped to the resonator are utilized to increase the tuning range of the distance between the passband frequencies. The measured data show that all circuits possess good in-band return losses and low insertion losses. In addition, all filters show an excellent rejection characteristic between each two adjacent passbands. The measured responses show good agreement with the simulated results.

REFERENCES

1. Behera, S. and K. J. Vinoy, "Microstrip square ring antenna for dualband operation," *Progress In Electromagnetics Research*, Vol. 93, 41–56, 2009.
2. Alkanhal, M. A. S., "Composite compact triple-band microstrip antennas," *Progress In Electromagnetics Research*, Vol. 93, 221–236, 2009.
3. Mokhtaari, M., J. Bornemann, K. Rambabu, and S. Amari, "Coupling-matrix design of dual and triple passband filters," *IEEE Trans. Microw. Theory Tech.*, Vol. 54, No. 11, 3940–3946, Nov. 2006.
4. Lee, J. and K. Sarabandi, "Design of triple-passband microwave filters using frequency transformation," *IEEE Trans. Microw. Theory Tech.*, Vol. 55, No. 1, 187–193, Jan. 2008.
5. Kuo, J.-T., T.-H. Yeh, and C.-C. Yeh, "Design of microstrip

bandpass filter with a dual-passband response," *IEEE Trans. Microw. Theory Tech.*, Vol. 53, No. 4, 1331–1337, Apr. 2005.

6. C.-F. Chen, T.-Y. Huang and R.-B. Wu, "Design of dual- and triple-passband filters using alternatively cascade multiband resonators," *IEEE Trans. Microw. Theory Tech.*, Vol. 54, No. 9, 3350–3358, Sep. 2006.
7. Chen, X. P., K. Wu, and Z.-L. Li, "Dual-band and triple-band substrate integrated waveguide filters with Chebyshev and quasi-elliptic responses," *IEEE Trans. Microw. Theory Tech.*, Vol. 55, No. 11, 2569–2578, Dec. 2007.
8. Yang, R.-Y., H. Kuan, C.-Y. Hung, and C.-S. Ye, "Design of dual-band bandpass filters using a dual feeding structure and embedded uniform impedance resonators," *Progress In Electromagnetics Research*, Vol. 105, 93–102, 2010.
9. Velazquez-Ahumada, M. D. C., J. Martel-Villagr, F. Medina, and F. Mesa, "Application of stub loaded folded stepped impedance resonators to dual band filter design," *Progress In Electromagnetics Research*, Vol. 102, 107–124, 2010.
10. Mo, S.-G., Z.-Y. Yu, and L. Zhang, "Design of triple-mode bandpass filter using improved hexagonal loop resonator," *Progress In Electromagnetics Research*, Vol. 96, 117–125, 2009.
11. Zhang, L., Z.-Y. Yu, and S.-G. Mo, "Novel planar multimode bandpass filters with radial-line stubs," *Progress In Electromagnetics Research*, Vol. 101, 33–42, 2010.
12. Menzel, W., L. Zhu, K. Wu, and F. Bogelsack, "On the design of novel compact broad-band planar filters," *IEEE Trans. Microw. Theory Tech.*, Vol. 51, No. 2, 364–370, Feb. 2003.
13. Chiou, Y.-C., J.-T. Kuo, and E. Cheng, "Broadband quasi-Chebyshev bandpass filters with multimode stepped-impedance resonators (SIRs)," *IEEE Trans. Microw. Theory Tech.*, Vol. 54, No. 8, 3352–3358, Aug. 2006.
14. Kuo, J.-T., Y.-C. Chiou, and E. Cheng, "High selectivity ultra-wideband (UWB) multimode stepped-impedance resonators (SIRs) bandpass filter with two-layer broadside-coupled structure," *Asia-Pacific Microwave Conference*, 2361–2364, Bangkok, Thailand, Dec. 2007.
15. Wong, S. W. and L. Zhu, "Implementation of compact UWB bandpass filter with a notch-band," *IEEE Microw. Wireless Compon. Lett.*, Vol. 18, No. 1, 10–12, Jan. 2008.
16. Chiou, Y.-C., Y.-F. Lee, C.-C. Chen, and J.-T. Kuo, "Planar multimode resonator bandpass filters with sharp transition and

wide stopband," *IEEE MTT-S Int. Microw. Symp. Dig.*, Atlanta, GA, USA, Jun. 2008.

17. Huang, T.-H., H.-J. Chen, C.-C. Chang, L.-S. Chen, Y.-H. Wang, and M.-P. Houng, "A novel compact ring dual-mode filter with adjustable second pass-band for dual-band applications," *IEEE Microw. Wireless Compon. Lett.*, Vol. 16, No. 6, 360–362, Jun. 2006.
18. Zhang, X. Y. and Q. Xue, "Novel dual-mode dual-band filters using coplanar-waveguide-fed ring resonators," *IEEE Trans. Microw. Theory Tech.*, Vol. 55, No. 10, 2183–2190, Oct. 2007.
19. Lugo, C. and J. Papapolymerou, "Multilayer dual-band filter using a reflector cavity and dual-mode resonators," *IEEE Microw. Wireless Compon. Lett.*, Vol. 17, No. 9, 637–639, Sep. 2007.
20. Liu, Y., W.-B. Dou, and Y.-J. Zhao, "A tri-band bandpass filter realized using tri-mode T-shape branches," *Progress In Electromagnetics Research*, Vol. 105, 425–444, 2010.
21. Matthaei, G. L., L. Young, and E. M. T. Jones, *Microwave Filters, Impedance-Matching Network, and Coupling Structures*, Sec. 11.02 $\sim$ 11.03, Artech House, Norwood, MA, 1980.
22. Zeland Software Inc., IE3D Simulator, Jan. 1997.
23. Kuo, J.-T., S.-P. Chen, and M. Jiang, "Parallel-coupled microstrip filters with over-coupled end stages for suppression of spurious responses," *IEEE Microw. Wireless Comp. Lett.*, Vol. 13, No. 10, 440–442, Oct. 2003.
24. Kuo, J.-T. and M.-H. Wu, "Corrugated parallel-coupled line bandpass filters with multispurious suppression," *IET — Microw. Antennas Propag.*, Vol. 1, No. 3, 718–722, Jun. 2007.
25. Velázquez-Ahumada, M. D. C., J. Martel, and F. Medina, "Parallel coupled microstrip filters with ground-plane aperture for spurious band suppression and enhanced coupling," *IEEE Trans. Microw. Theory Tech.*, Vol. 52, 1082–1086, Mar. 2004.
26. Kuo, J.-T. and E. Shih, "Wideband bandpass filter design with three-line microstrip structures," *Proc. Inst. Elect. Eng.*, Part H, Vol. 149, No. 5, 243–247, Oct. 2002.